

Introduction & Observations

Date YY-MM-DD	S_{tot} [Jy]			Beam (bpa), [μas] \times [μas] ($^{\circ}$)			Missing Antennas
	23 GHz	43 GHz	86 GHz	23 GHz	43 GHz	86 GHz	
2017-06-27	4.04	5.53	0.91	630 \times 340 (-3)	340 \times 200 (0)	27 \times 120 (-8)	
2017-07-31	3.95	4.62	1.17	580 \times 290 (-5)	330 \times 180 (-4)	280 \times 80 (-19)	FD
2017-08-29	3.96	4.93	0.52	600 \times 350 (-2)	340 \times 200 (3)	660 \times 580 (51)	
2017-09-25	4.23	4.52	0.70	850 \times 380 (-16)	470 \times 230 (-16)	310 \times 230 (-20)	SC
2018-02-12	5.08	3.91	0.68	850 \times 440 (-12)	490 \times 240 (-12)	350 \times 300 (42)	HN, SC
2018-04-06	4.24	4.35	n/a	660 \times 340 (-8)	370 \times 200 (2)	n/a	
2018-05-18	4.34	4.29	0.75	1010 \times 430 (-14)	380 \times 200 (3)	400 \times 330 (-4)	HN
2018-06-09	4.25	3.89	n/a	660 \times 360 (9)	380 \times 210 (10)	n/a	
2018-07-04	4.01	3.92	0.30	600 \times 310 (-3)	330 \times 180 (-1)	200 \times 90 (-13)	PT
2018-08-28	5.07	2.44	0.50	840 \times 420 (-13)	350 \times 220 (10)	310 \times 270 (71)	

Tab. 1: Summary of VLBA observations.

The flat spectrum radio quasar (FSRQ) 3C 345 ($z=0.595$, 6.64 pc/mas) is a well-monitored blazar from the gamma rays to radio wavelengths. The curved compact jet contains multiple apparently superluminal components. Schinzel et al. (2012) showed that during a flaring state, component ejection triggers gamma ray emission. More recently, Pötzl et al. (2021) uncovered new polarized components and magnetic field structure from RadioAstron space VLBI images.

The primary goal of this project is to use the observed polarized emission at 23, 43 and 86 GHz to trace the magnetic field structure of the compact jet. So far, we have analyzed the total intensity structure of the compact jet and the kinematics of the robustly cross-identified components.

The Project

Total intensity maps:

- core shift measurement
- spectral index maps
- synchrotron turnover maps

Polarized emission:

- magnetic field structure
- Faraday rotation measure

To model and interpret our measurements, we will employ radiative special-relativistic magneto-hydrodynamic simulations reproducing the structure and emission of the compact jet. The measurements listed above will help us to uniquely constrain our simulation parameters and to probe the evolution of the underlying physical processes. For instance, mapping the spectral index shows directly where electrons suffer synchrotron losses due to strong magnetic fields, expected in regions where the jet re-collimates. Changes in the jet geometry may allow us to estimate spin of the central black hole, and the core shift holds information about the magnetic field strength (Nokhrina et al. 2020, Ricci et al. 2022).

Total Intensity parsec-scale Structure

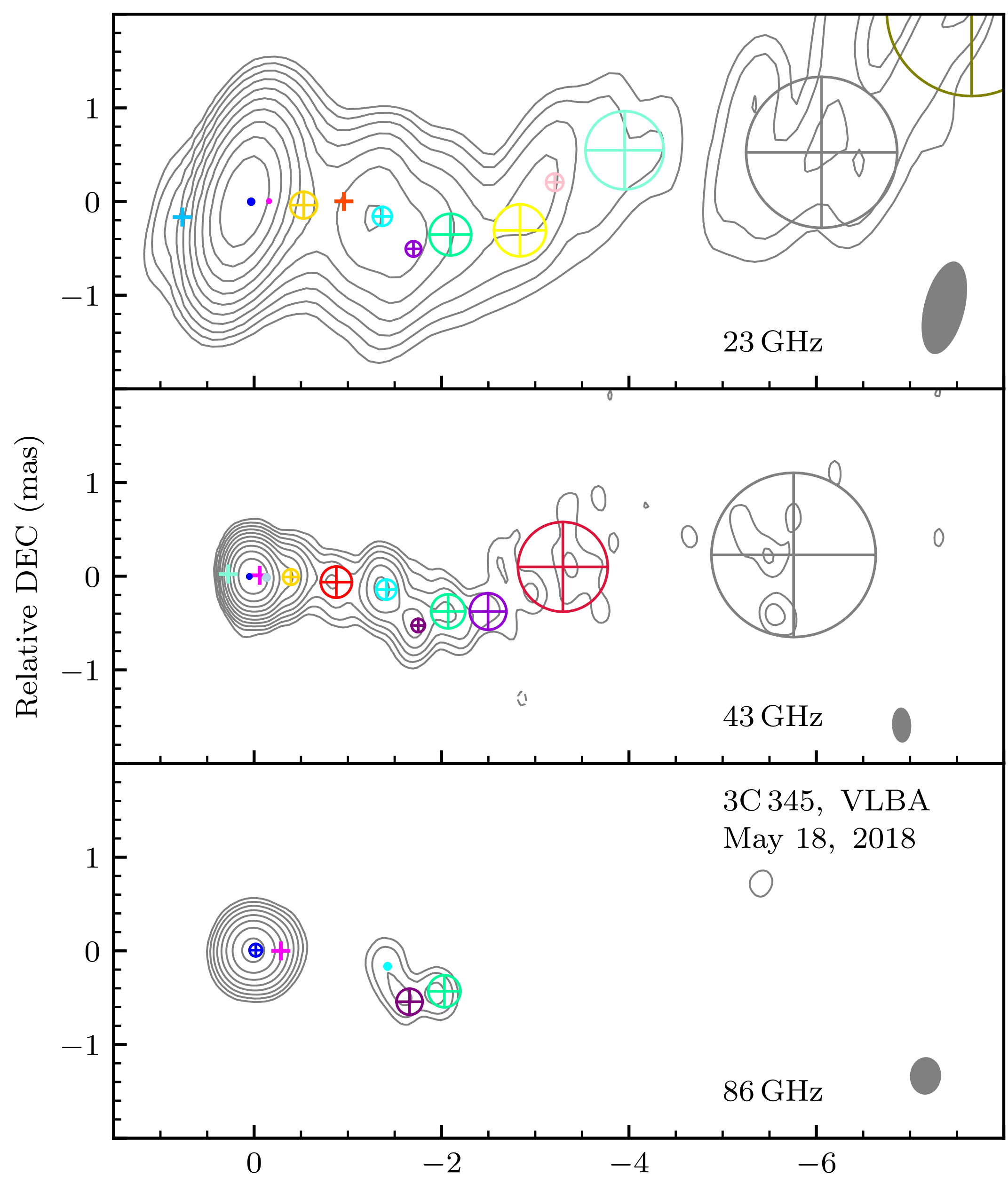


Fig. 1: CLEAN images of the total intensity radiation in the jet of 3C 345 at 22, 43 and 86 GHz. Contour levels start at 0.1% of the peak flux for the top two, and at 0.6% of the peak for the bottom panel. Circular Gaussian model fit components are overplotted, with color coding added to aid cross-identification. The restoring beam is shown in the bottom right corner.

We model the 23 GHz and 43 GHz total intensity structure with sometimes more than ten circular Gaussian components, eight of which can be robustly cross-identified at multiple consecutive epochs. The compact jet shows the well-known strong curvature and knotty structure.

43 GHz Jet Kinematics

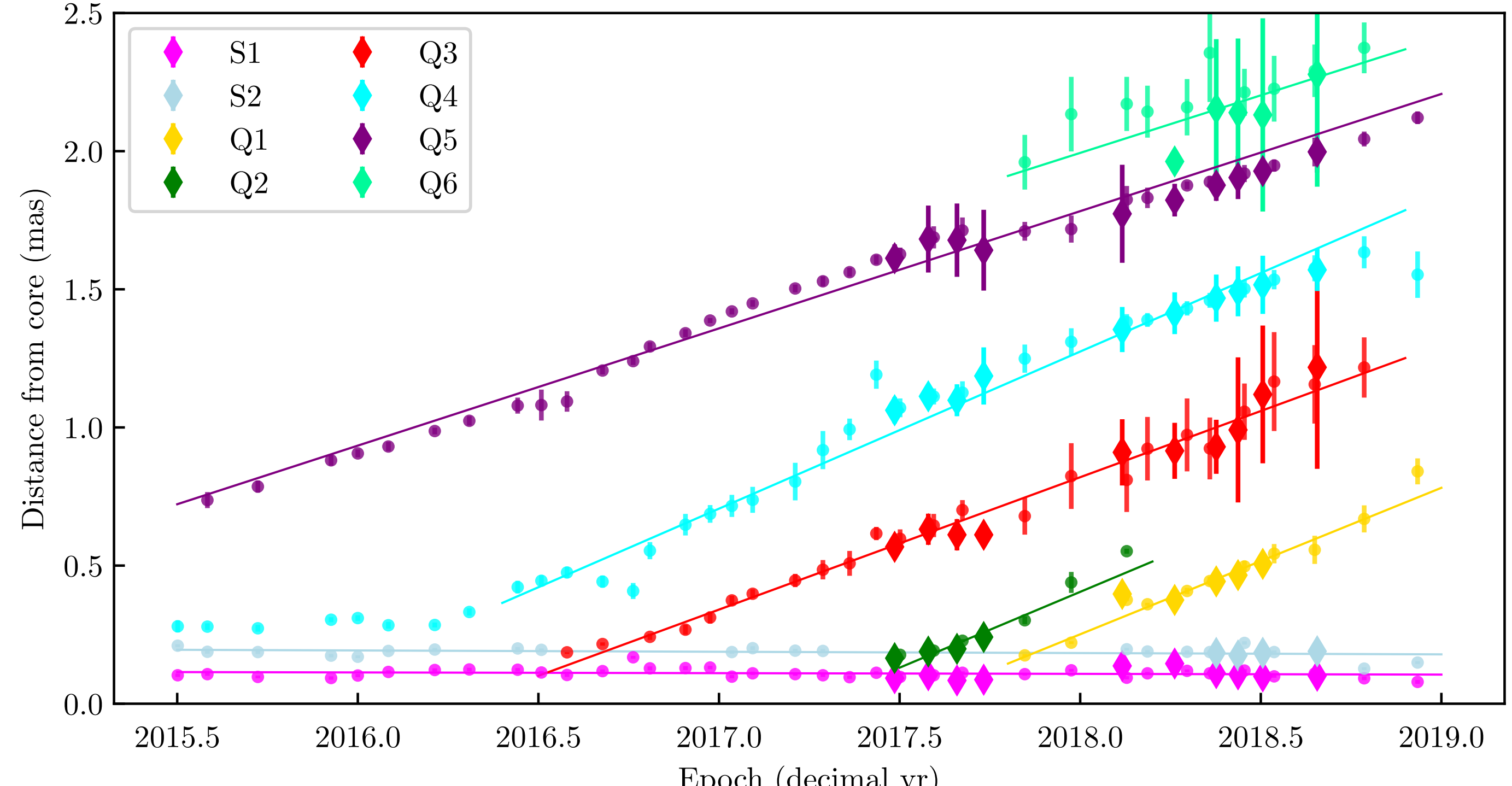


Fig. 2: Core separation of robustly detected components in the 3C 345 jet at 43 GHz approximated by linear fits. Diamonds: measurements from this study. Circles: results by Weaver et al. (2022), shown together to increase the robustness of the fits.

Label	Q1	Q2	Q3	Q4	Q5	Q6
#	16	10	34	38	45	15
$\langle \mu \rangle$ [mas/yr]	0.53 ± 0.03	0.55 ± 0.07	0.48 ± 0.01	0.57 ± 0.01	0.42 ± 0.01	0.42 ± 0.11
$\langle \beta_{\text{app}} \rangle$ [c]	18.29 ± 1.19	18.9 ± 2.4	16.50 ± 0.5	19.6 ± 0.5	14.64 ± 0.28	14.0 ± 4.0
δ_{var}^*	18.0 ± 3.0	18.7 ± 2.5	22.0 ± 2.8	2.2 ± 0.9	5.2 ± 0.8	103.9 ± 37.8
Γ_{var}^*	20.2 ± 1.9	20.3 ± 2.8	16.7 ± 0.8	58.0 ± 23.0	24.0 ± 3.0	53.0 ± 19.0

Tab. 3: Measured apparent speeds from the fits shown in Fig. 2. We exclude the stationary components S1 and S2 for clarity. *Variability Doppler and Lorentz factors taken from Weaver et al. (2022), pending an update based on this study.

We identify two stationary (S1 and S2) and six superluminally moving components (Q1–Q6). Newly ejected components apparently pass through S2, consistent with a standing shock. None of the newly ejected components accelerate, in contrast to those ejected during the flaring state of 3C 345 discussed by Schinzel et al. (2012).

Radio and Gamma Ray Light Curves

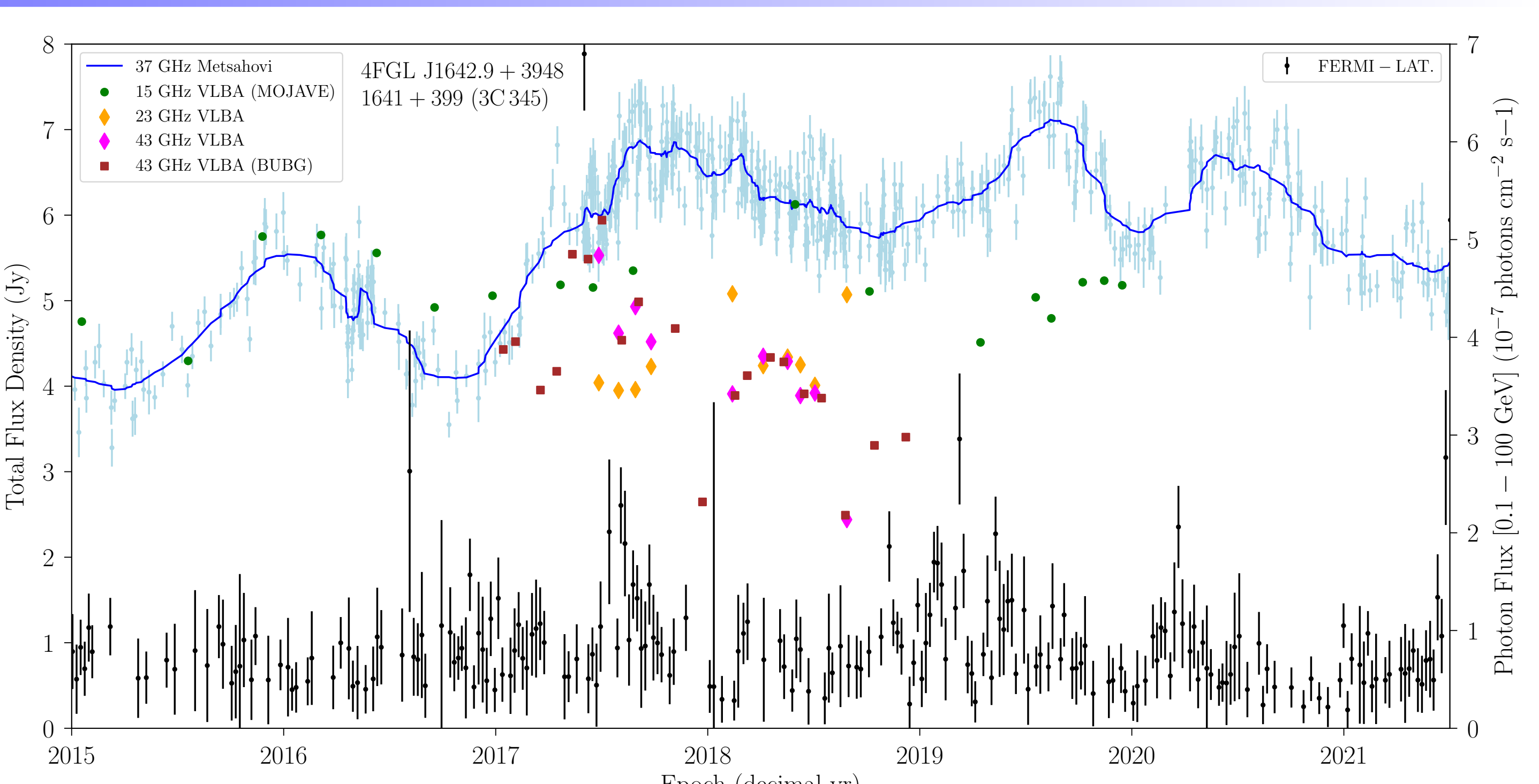


Fig. 3: Variability properties of 3C 345. Total flux density of radio emission at 37 GHz (blue; Aalto U. Metsähovi Observatory, priv. comm.) is approximated by a Savitzky-Golay filter (solid line). Total flux densities of VLBI structures at 15 GHz (green circles), 23 GHz (orange diamonds), and 43 GHz (pink diamonds and brown squares) are shown for comparison, with diamonds indicating our new measurements. In black: FERMI/LAT gamma ray light curve (Kocevski et al. 2021).

To complement our VLBI measurements, we show the variability properties of 3C 345 in Fig. 3. Schinzel et al. (2012) showed that relativistic outflow drives the gamma ray emission, and indeed we see a spike in the gamma rays towards the end of 2017, after the ejection of Q2 and Q3.

References

- Kocevski, D. and Fermi Large Area Telescope Collaboration, 2021, The Astronomer's Telegram, 15110:1
- Nokhrina, E. E., Kovalev, Y. Y. and Pushkarev, A. B. 2020, MNRAS, 498, 2, 2532
- Pötzl, F. M., Lobanov, A. P., Ros, E., et al. 2021, A&A, 648, A82
- Ricci, L., Boccardi, B., Nokhrina, E. E. et al. 2022, eprint arXiv:2206.12193, A&A in press
- Schinzel, F. K., Lobanov, A. P., Taylor, G. B., et al. 2012, A&A, 537, A70
- Weaver, Z. R., Jorstad, S. G., Marscher, A. P., et al. 2022, ApJ, 260, 1, 12, 42
- additional material: —
- Biretta, J. A., Moore, R. L. and Cohen, M. H. 1986, ApJ, 308, 93
- Lobanov, A. P. and Zensus, J. A. 1999, ApJ, 521, 509
- Lobanov, A. P. and Roland, J. 2005, A&A, 431, 831
- Ros, E., Zensus, J. A. and Lobanov, A. P. 2000, A&A, 354, 55
- Zensus, J. A., Cohen, M. H. and Unwin, S. C. 1995, ApJ, 443, 35
- Steffen, W., Zensus, J. A., Krichbaum, T. P. et al. 1995, A&A, 302, 335